Turkish Journal of Electrical Engineering & Computer Sciences

http://journals.tubitak.gov.tr/elektrik/

Research Article

Turk J Elec Eng & Comp Sci
(2018) 26: 1515 – 1529

doi:10.3906/elk-1605-356

Conception and control of a WTGS system using a novel control technique based on MPC-DPC-MVF with a switch optimization process

Mansour MADACI*, Djallel KERDOUN
LGEC – Research Laboratory, Department of Electrical Engineering, Constantine 1 University, Constantine, Algeria

Received: 30.05.2016 • **Accepted/Published Online:** 06.06.2017 • **Final Version:** 30.05.2018

Abstract: The work proposed through this paper presents a novel technique applied for the control of a wind turbine generation system (WTGS) prototype. A model predictive control combined with a direct power control technique (MPC-DPC) based on SVM control and a novel switching cycle sequence pattern for thermal switch losses reduction have been adopted. The novel developed direct power control (DPC) scheme based on a multivariable filter (MVF) topology for power estimation process has been illustrated. The control of the converter system is adopted through a predictive control strategy to achieve a complete and an instantaneous control over the active and the reactive powers flowing from and to the converter. An experimental implementation has been achieved for the validation of the system using both real-time simulation mode and a full control system with hardware synchronization mode. A switches losses modelling was achieved to evaluate the performances of the proposed control technique.

Key words: Wind turbine generation system, MPC-DPC control technique, SVM control technique, switches cycle sequence pattern table, multivariable filter topology, instantaneous active and reactive power control, wind chain buck to buck power electronic converter, FPGA system control implementation, real-time control system, thermal switches losses modelling

1. Introduction

By the end of the 60s, the evolution of power electronic converters and control platforms based on DSPs and FPGAs allowed research to takes a new way in the control of electric power and power machinery control. The integration of the control techniques became possible from theory to reality. This leads to a deep investigation on the electrical control domain and its applications. New control techniques appear, others have been improved, and the application of new ideas became possible.

The model predictive control (MPC) topology has been widely used in conjunction with new drivers [1–4]; this control technique offers many advantages mainly due to its simplicity and reliability face of the parameters' uncertainty and variation. Predictive control appears as an alternative issue for the control of power converters as a fast dynamic solution with easy implementation.

The main scheme of the technique reflects on the use of the system model to predict the behavior of the variable and its possible changes over certain horizon time starting from the current system state using the state space of the system itself. A cost effective function is applied as a criterion for the optimum future decision selection over the predetermined horizon [5,6]. The decision comes by selecting the most suitable switching state applied to the converter for the desired output value obtainment. For this purpose, a novel switch pattern has

*Correspondence: zoldaioque@gmail.com

been proposed regarding thermal losses minimization of the power electronic modules constructing the converter system; the principle is that one switch changes its state from a vector to another or from a sector to another. The application of the zero vectors allows a wide range of control over the DC bus voltage.

The authors in this work have investigated the use of a multivariable filter (MVF) model to extract the fundamental reference of the virtual flux starting from the voltage vector and the applied a switches sequence pattern. The MVF control technique topology is widely used in power quality improvement mainly through power active filter structures [7–15].

The switches' losses have been modelled to evaluate the proposed control technique applied on the rectifier stage and its effect on the converter performances. This leads to the improvement of the cooling system determination to be installed and to optimize the size of the converter and improves its performances.

2. WTGS power train converter control system topology

2.1. Rectifier control technique using DPC-MVF with switches sequence pattern optimization and input filter stage design

The active power for a three phase power system is determined by the scalar product between the system voltages and currents. The vector product gives the system reactive power term.

$$p = v_a i_a + v_b i_b + v_c i_c \tag{1}$$

$$q = \frac{1}{\sqrt{3}} \left[(v_a - v_c) i_a + (v_c - v_a) i_b + (v_a - v_b) ic \right] \tag{2}$$

For a sinusoidal and balanced line voltage on the rectifier input side of WTG system, the derivative of the flux component amplitudes is null. The expressions of both the active and reactive powers can be represented through the virtual component of the flux term by

$$p = w(\psi_{L\alpha} i_{L\beta} - \psi_{L\beta} i_{L\alpha}) \tag{3}$$

$$q = w(\psi_{L\alpha} i_{L\alpha} - \psi_{L\beta} i_{L\beta}) \tag{4}$$

$$\psi_L = \int U_L dt \tag{5}$$

since

$$U_L = \begin{bmatrix} U_{L\alpha} \\ U_{L\beta} \end{bmatrix} = \sqrt{\frac{2}{3}} \begin{bmatrix} 1 & \frac{1}{2} \\ 0 & \sqrt{\frac{3}{2}} \end{bmatrix} \begin{bmatrix} U_{ab} \\ U_{bc} \end{bmatrix} \tag{6}$$

$$\psi_L = \begin{bmatrix} \psi_{L\alpha} \\ \psi_{L\beta} \end{bmatrix} = \begin{bmatrix} \int U_{L\alpha} dt \\ \int U_{L\beta} dt \end{bmatrix} \tag{7}$$

$$U_{s\alpha} = \sqrt{\frac{2}{3}} Udc(sa + \frac{1}{2}(sb + sc) \tag{8}$$

$$U_{s\beta} = \frac{1}{\sqrt{2}} Udc(sb - sc) \tag{9}$$

For a sampling period Ts is assumed to be small enough compared to the system power source voltage period. The quantities $U\alpha\beta\,(k+1) = U\alpha\beta(k)$. Hence, $\psi\alpha\beta\,(k+1) = \psi\alpha\beta(k)$. With $U\alpha\beta, \psi\alpha\beta$: are the voltage and the flux components on the $(\alpha\beta)$ frame.

Then the variation in the active and reactive powers within successive discrete sampling periods can be expressed through the following equations:

$$[p(k+1) - p(k)] = w\,[(\psi_{L\alpha}(i_{L\beta}(k+1) - i_{L\beta}(k)) - \psi_{L\beta}(i_{L\alpha}(k+1) - i_{L\alpha}(k))] \tag{10}$$

$$[Q(k+1) - Q(k)] = w\,[\psi_{L\alpha}(i_{L\alpha}(k+1) - i_{L\alpha}(k)) - \psi_{L\beta}(i_{L\beta}(k+1) - i_{L\beta}(k))] \tag{11}$$

Eqs. (10) and (11) successively illustrated above give the evolution of the active and reactive power system variations regarding the variation in both system quantities applied: the virtual estimated flux and the currents system.

The DPC control technique scheme (Figure 1) consists of controlling the two quantities of the active and reactive powers by applying a predefined switching state sequence to the gates of the IGBTs converter device with the aim of ensuring full control over the two output quantities within the desired references. Eqs. (8) and (9) demonstrate that the switches state applied to this latter could be used for the estimation of the output system voltage variation. This leads to no need for the use of a voltage measurement probe and minimizes the complexity of the system implementation process. The flux component variation is obtained by integrating the voltage quantities on the alpha beta frame as illustrated through Eq. (7).

Instead of applying the traditional commonly used method for virtual flux components estimation, a MVF has been adopted looking to its robustness during the real-time execution process with fast implementation. Initially, its basic principal is the extraction of the fundamental component of the flux directly on the $\alpha\beta$ axes.

Expressions linking the output component $\hat{X}\alpha\beta$ of the multivariable filter system to the $X\alpha\beta$ components (X being the main flux input) are illustrated below

$$\hat{X}_\alpha = \frac{k}{s}\left[X_\alpha(s) - \hat{X}_\alpha(s)\right] - \frac{\omega_c}{s}X_\beta(s) \tag{12}$$

$$\hat{X}_\beta = \frac{k}{s}\left[X_\beta(s) - \hat{X}_\beta(s)\right] - \frac{\omega_c}{s}X_\alpha(s) \tag{13}$$

ω_c : The cut-off frequency of the filter
k : Constant gain
$\omega_c = n.\varepsilon.\omega_f$ With:ε: constant gain ± 1 ($+1$ for the direct component, –1 for the reverse component), n: the order of the harmonic to be eliminated.

The diagram block for the proposed method is illustrated in the figure below (Figure 2).

The authors propose in this work a novel switching sequence control topology that consists of reorganizing the application of the zero vectors position state regarding the active vectors control switches position on the base that one switch at most changes its state from a vector to another. This minimizes the high frequency commutation, which reduces the IGBTs junction thermal dissipation.

The switching state sequences for the different sectors applied to the rectifier stage are illustrated below (Table 1).

Since the rectifier stage of the power train conversion system is considered as a current source, the installation of a passive filter is necessary to attenuate the distortions due to the IGBTs high switching rate

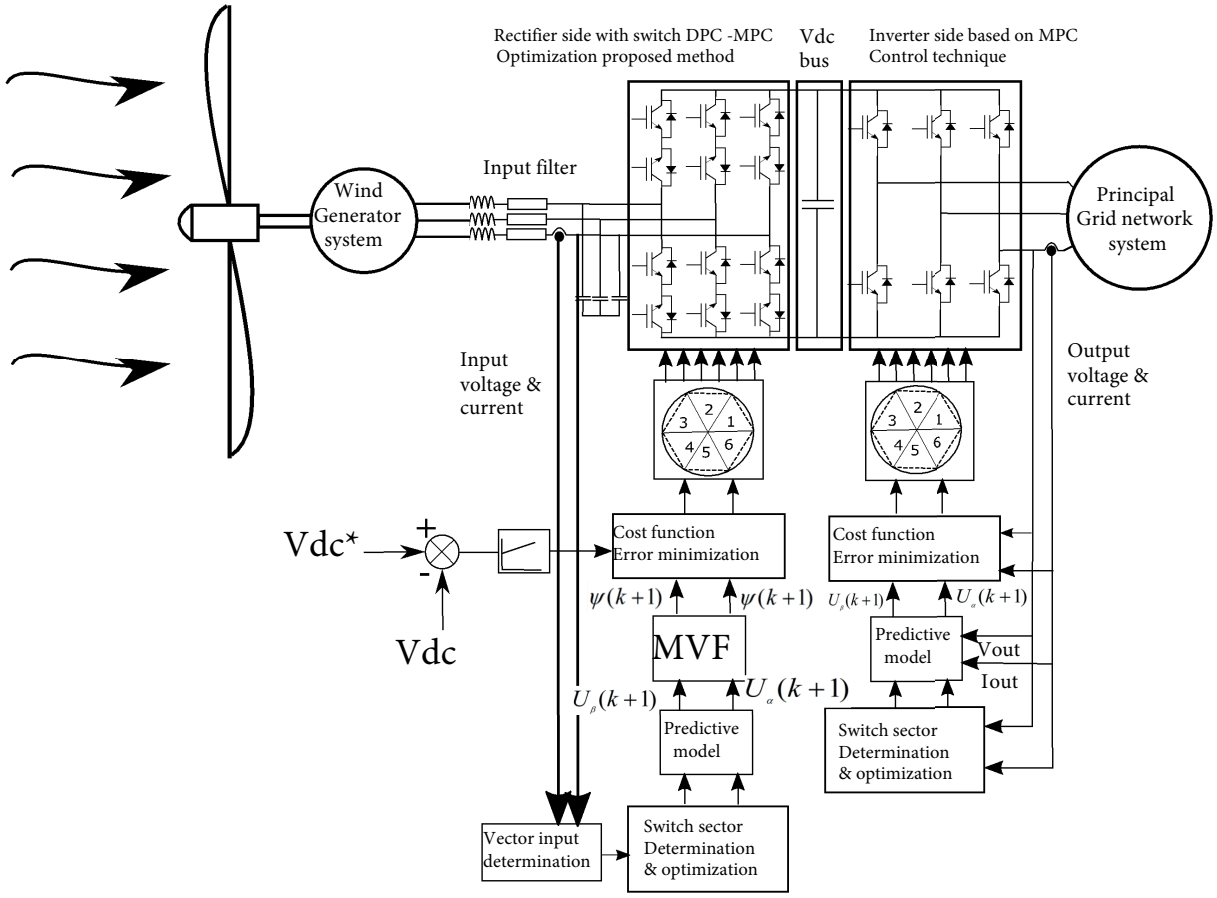

Figure 1. Block diagram for the WTGS based on MPC-DPC control using MVF technique.

commutation; this improves the current quality in the input side of the converter and avoids the propagation of commutations effect from the converter to the main grid.

The characteristics of the adopted LC filter have been studied and both the magnitude and phase diagrams have been illustrated (Figure 3). The filter capacitor value is essential in the determination of the size and affects directly the input power factor value of the system; with the high capacitor value high displacement on the power factor (PF) appears. Hence, this latter should be minimized. A work has been presented by Vlatkovic et al. [16] giving the maximum value for the capacitor to be installed.

$$C\max = \frac{Im}{\omega Vm}(\cos^{-1} IDF), \tag{14}$$

where Im and Vm are the maximum input current and the maximum input voltage respectively, ω is the angular frequency, and IDF is input displacement factor.

2.2. WTGS inverter side predictive control

Considering the inverter stage of the WTGS converter system as a standalone inverter (Figure 4), for a set of given three phase sinusoidal input voltages system

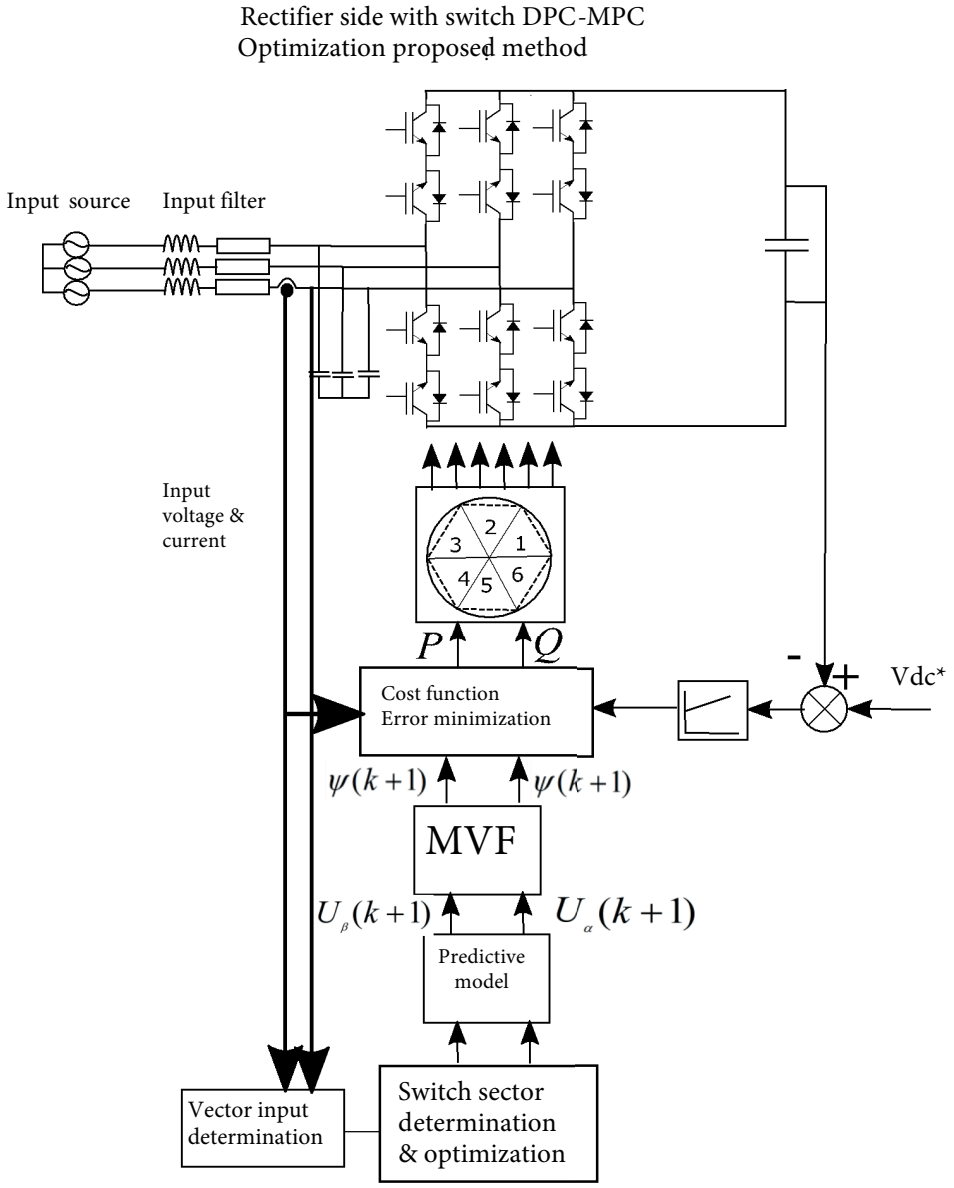

Figure 2. Block diagram for the MPC DPC PWM rectifier side of the converter.

$$\begin{bmatrix} Van \\ Vbn \\ Vcn \end{bmatrix} = V_{outm} \begin{bmatrix} \cos(w_{out}t) \\ \cos(w_{out}t - 120°) \\ \cos(w_{out}t + 120°) \end{bmatrix} \tag{15}$$

The state space of the previous equation demonstrating the output voltage system generated by the inverter is given by

$$V = \frac{2}{3}(Van + aVbn + a^2Vcn) \tag{16}$$

The inverter side output voltage system is provided by the DC link system controlled around 360° with Sa, Sb, Sc representing successively the three upper legs of the inverter and providing the three output voltages Van,

Table 1. The proposed switching state including zero vectors for the rectifier stage.

Sa	$\overline{Sa}$	Sb	$\overline{Sb}$	Sc	$\overline{Sc}$	Sa	$\overline{Sa}$	Sb	$\overline{Sb}$	Sc	$\overline{Sc}$
1	**1**	**0**	**0**	**0**	**0**	**0**	**0**	**0**	**0**	**1**	**1**
1	0	0	1	0	0	1	0	0	0	0	1
0	**0**	**1**	**1**	**0**	**0**	**1**	**1**	**0**	**0**	**0**	**0**
1	0	0	0	0	1	0	0	0	1	0	1
0	**0**	**0**	**0**	**1**	**1**	**0**	**0**	**1**	**1**	**0**	**0**
Sector I Sector II											
0	**0**	**1**	**1**	**0**	**0**	**1**	**1**	**0**	**0**	**0**	**0**
0	0	1	0	0	1	0	1	1	0	0	0
0	**0**	**0**	**0**	**1**	**1**	**0**	**0**	**1**	**1**	**0**	**0**
0	1	1	0	0	0	0	1	0	0	1	0
1	**1**	**0**	**0**	**0**	**0**	**0**	**0**	**0**	**0**	**1**	**1**
Sector III Sector IV											
0	**0**	**0**	**0**	**1**	**1**	**0**	**0**	**1**	**1**	**0**	**0**
0	1	0	0	1	0	0	0	0	1	1	0
1	**1**	**0**	**0**	**0**	**0**	**0**	**0**	**0**	**0**	**1**	**1**
0	0	0	1	1	0	1	0	0	1	0	0
0	**0**	**1**	**1**	**0**	**0**	**1**	**1**	**0**	**0**	**0**	**0**
Sector V Sector VI											

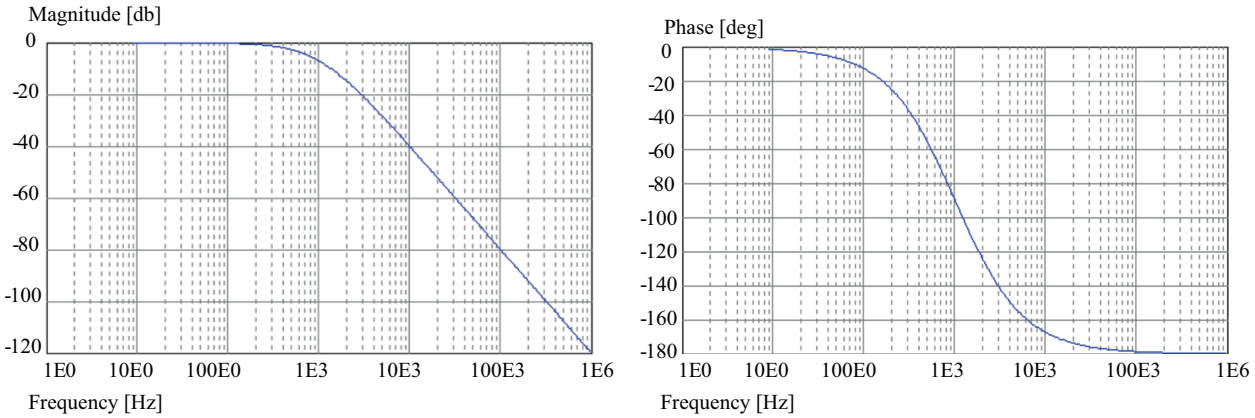

Figure 3. Input installed filter characteristics using phase and magnitude diagrams.

Vbn, Vcn:

$$V = Vdc.S(a,b,c) \tag{17}$$

Hence, $S(a,b,c) = \frac{2}{3}(Sa + a.Sb + a^2.Sc)$

The load current dynamic variation for the inverter stage can be expressed by

$$V = Ri + L\frac{di}{dt} + e \tag{18}$$

For the demonstration of the sampling period Ts representing the load current variations on a rated period

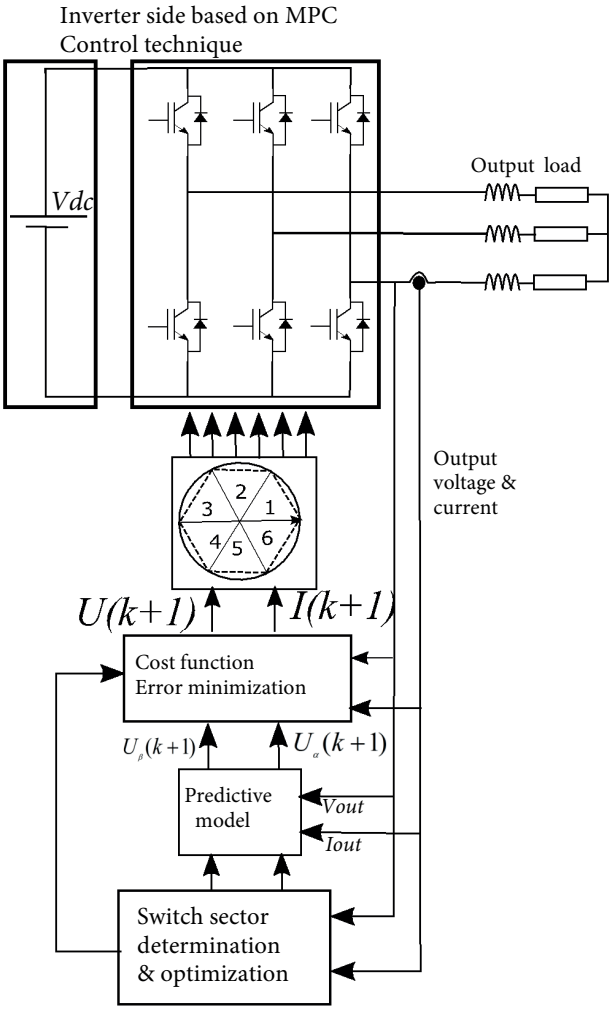

Figure 4. Block diagram for the MPC inverter side of the converter system.

smaller than the current output one the current variation could be approximated by

$$\frac{di}{dt} = \frac{i(k+1) - i(k)}{Ts} \tag{19}$$

The discrete dynamic variation of the future load current value i(k+1) from its previous value i(k) for a sampling period Ts is expressed by

$$i(k+1) = \frac{1}{R.Ts + L}(L.i(k) + Ts.V(k+1) - Ts.e(k+1) \tag{20}$$

Table 2 summarizes the inverter control topology regarding the switches position determining the voltage output vector for the future load current prediction.

For the instant when the reference Vout* is determined, a PLL is used to classify the position of the input reference to the appropriate sector it belongs. The switching sequences appropriate for that reference sector are applied to control the output voltage.

Table 2. Switching state related to the vector voltages for the output inverter system.

Sa	Sb	Sc	$\overline{Sa}$	$\overline{Sb}$	$\overline{Sc}$	Vk	Va	Vb	Vc
0	0	0	1	1	1	V0	0	0	0
1	0	0	0	1	1	V1	$0.66Vdc$	$-0.33Vdc$	$-0.33Vdc$
1	1	0	0	0	1	V2	$0.33Vdc$	$0.33Vdc$	$-0.66Vdc$
0	1	0	1	0	1	V3	$-0.33Vdc$	$0.66Vdc$	$-0.33Vdc$
0	1	1	1	0	0	V4	$-0.66Vdc$	$0.33Vdc$	$0.33Vdc$
0	0	1	1	1	0	V5	$-0.33Vdc$	$-0.33Vdc$	$0.66Vdc$
1	0	1	0	1	0	V6	$0.33Vdc$	$-0.66Vdc$	$0.33Vdc$
1	1	1	0	0	0	V7	0	0	0

An optimized table has been proposed by the authors to handle a performed controlled system. The main principal has been discussed above for the rectifier stage control process.

The table (Table 3) below gives the combination of the switching sequence used within the six sectors for the inverter control

Table 3. The proposed switching state including zero vectors for the inverter stage.

Sa	$\overline{Sa}$	Sb	$\overline{Sb}$	Sc	$\overline{Sc}$	Sa	$\overline{Sa}$	Sb	$\overline{Sb}$	Sc	$\overline{Sc}$
1	0	0	1	0	1	1	0	1	0	0	1
1	0	1	0	0	1	0	1	1	0	0	1
1	**0**	**1**	**0**	**1**	**0**	**0**	**1**	**0**	**1**	**0**	**1**
1	0	1	0	0	1	0	1	1	0	0	1
1	0	0	1	0	1	1	0	1	0	0	1
Sector I Sector II											
0	1	1	0	0	1	0	1	1	0	1	0
0	1	1	0	1	0	0	1	0	1	1	0
1	**0**	**1**	**0**	**1**	**0**	**0**	**1**	**0**	**1**	**0**	**1**
0	1	1	0	1	0	0	1	0	1	1	0
0	1	1	0	0	1	0	1	1	0	1	0
Sector III Sector IV											
0	1	0	1	1	0	1	0	0	1	1	0
1	0	0	1	1	0	1	0	0	1	0	1
1	**0**	**1**	**0**	**1**	**0**	**0**	**1**	**0**	**1**	**0**	**1**
1	0	0	1	1	0	1	0	0	1	0	1
0	1	0	1	1	0	1	0	0	1	1	0

3. Simulation and the obtained results discussion

The system model has been initially simulated with a high power range. Later, the real parameters for the different system parts available on the experimental bench have been fitted on the simulated model parameters and 7.5 kW IGBTs modules have been used to build both sides of the converter prototype. A 2 kHz cut

frequency LC passive components input filter with 28.5 μF capacitor value C_F, 1 mH for the inductance input L_F, and 29 Ω for the resistor has been installed. For the generator side, 4 poles 10.6 kW PMSM have been used as a power generator for the turbine system, with 0.165 Ω stator resistor, 4.45 mH inductance, and 16.83e^{-3} kg.m^2 inertia. A system limit of 5 kW range has been used as a border for our system as a supplementary protection issue.

The graphs illustrated below (Figure 5) give the three modules thermal simulation study and the different losses on the IGBT modules with their functionality temperature dissipation.

The total module heat thermal study is illustrated below (Figure 6) giving the internal temperature for the IGBT's modules' junctions.

A 10 to 14.5 m/s wind profile variation range has been used for the model simulation process (Figure 7). A system limitation of 5 kW has been applied regarding the IGBT power rate used on the experimental side as cited above. As the figures (Figures 8 and 9) illustrate, the adopted MPC-DPC method guarantees full control of the power flowing from the generator to the converter with a zero reactive power and unity power factor functionality system from both sides of the converter (Figures 10 and 11). To evaluate the capabilities of the proposed control scheme from one side and to minimize the harmonics propagation injected into the grid from another, the spectral analysis of the modulated current by the converter for 25 kHz frequency control is presented in Figure 12. On the other hand, the sector selection using the proposed MPC control regarding the desired reference has been illustrated in Figure 13. Figures 14 and 15 give both the voltage and the current output system provided by the inverter delivered to the grid. In our case, an RL load has been used to make a similarity between the simulation and the experimental bench with its programmable load from California Instruments. For the control of the inverter stage, the DPC-MPC technique carries the power rate transmitted from the rectifier to the DC bus through the inverter.

The estimated voltage system variation on the (α, β) frame shown in Figure 16 is estimated using the virtual flux component on the same frame (Figure 17).

The system model was initially studied with no input filter to check the model's performance. Figures 18 and 19 demonstrate the improvement of the energy quality before and after the installation of the designed filter during the simulation process.

An 8% THD with no input filter has been reduced to 4.12%. Figures 20 and 21 give the spectral analysis of the input currents before and after the filter installation.

4. System implementation and experimental results' discussion

Many steps have been followed for the system implementation process. For this purpose, the process takes two main ways: in the first stage, a real-time simulation model with software synchronization mode; then model implementation with hardware synchronization mode. It is essential to carry out simulations in real-time synchronization between the devices we use.

Real-time simulation is used in devices between the host PC and the FPGA development card with its output connection cards for the IGBTs gate control. This latter receives orders from an eMEGAsim RT LAB system (Figure 22) with a model implemented for the converter model that ensures synchronization between the devices using buffers in the input and the output of the system.

In the last stage of our experimental implementation of the rapid converter control prototyping, the built platform model based on the RT Lab eMEGAsim digital control prototype was connected to the FPGA development board that controls the IGBTs' drivers using the implemented dead time protocol. In addition, a

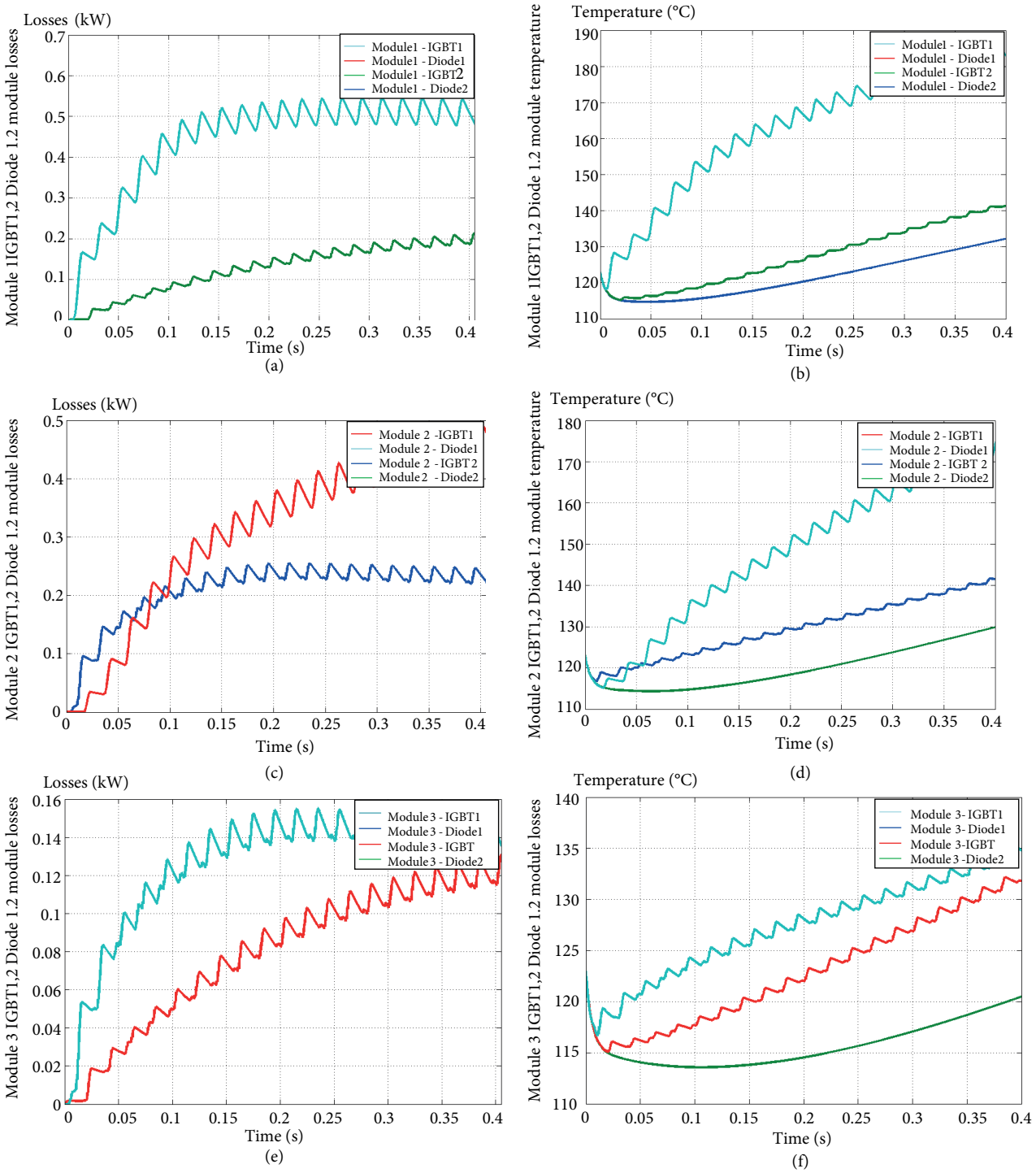

Figure 5. Power losses and junction temperature for the IGBT modules (IGBTs, diodes) on the rectifier side by applying the proposed method.

three-phase load of California 3091LD Programmable Instruments has been used to create the RL load for the power system. Later, the system has been divided into two FPGAs cards for the inverter with its MPC-DPC technique and proposed switches sequence table, where the other part was used for the control of the rectifier

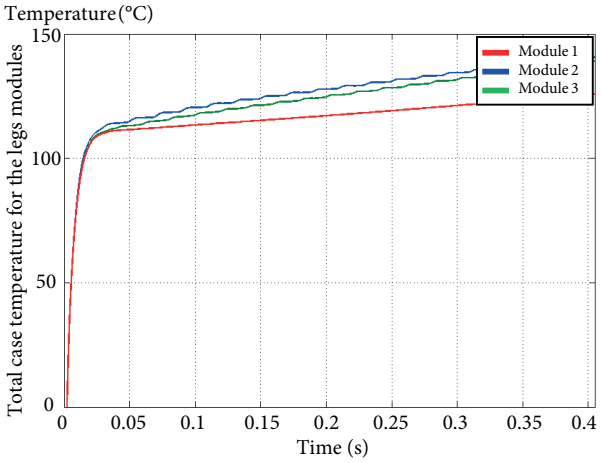

Figure 6. Total case temperature for the three legs modules.

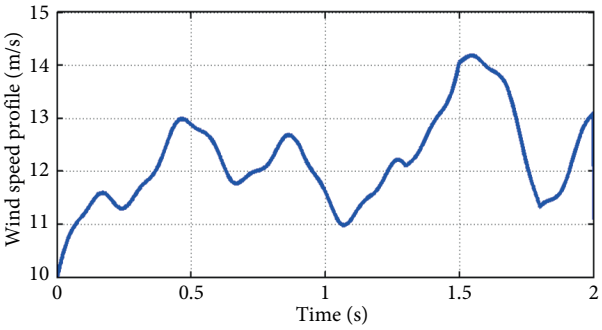

Figure 7. Applied wind speed profile.

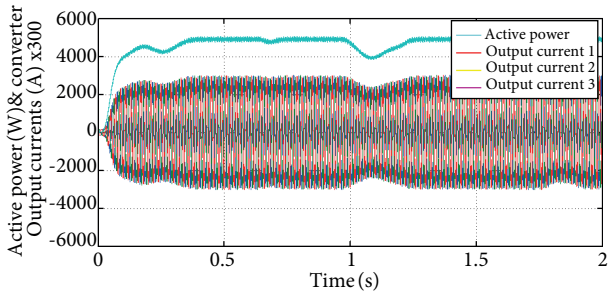

Figure 8. Active power control with rectifier input currents.

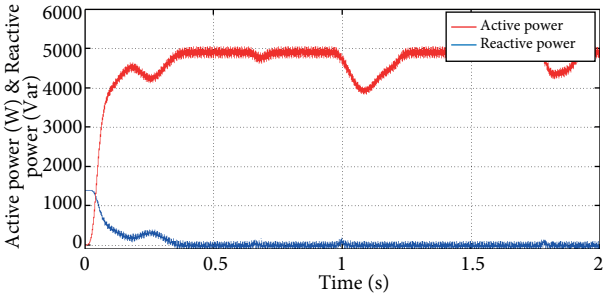

Figure 9. Controlled input active and reactive powers of the rectifier stage.

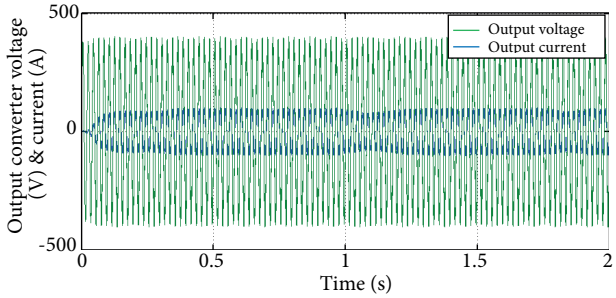

Figure 10. Input phase control for the system voltage and current.

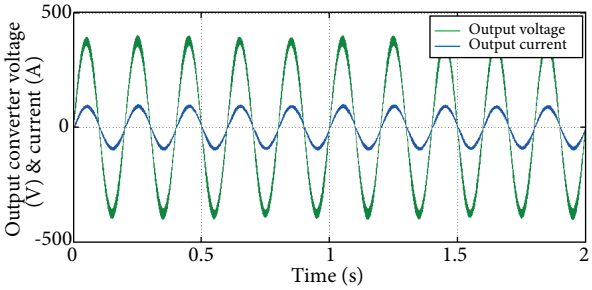

Figure 11. Zoom on the converters' input phase.

side (Figure 23). The purpose after this is to get the adequate execution time and to give the system high performances. The prototype is based on SPARTAN 6 FPGA with opto-isolated gate drivers MCP1407 from MICRISHIP for the drive of the IGBT modules.

A test was done for a single module controlled through an FPGA card with opto-isolated IGBT gate driver MCP1407 using high frequency around 25 kHz range with SVM technique (Figure 24) to validate the simulated results. A thermal camera has been used for this purpose to get the skinny temperature of the module (Figure 25).

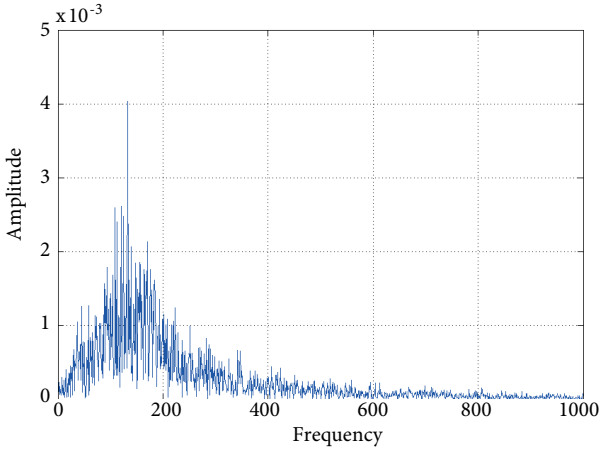

Figure 12. Spectral analysis of the input currents control.

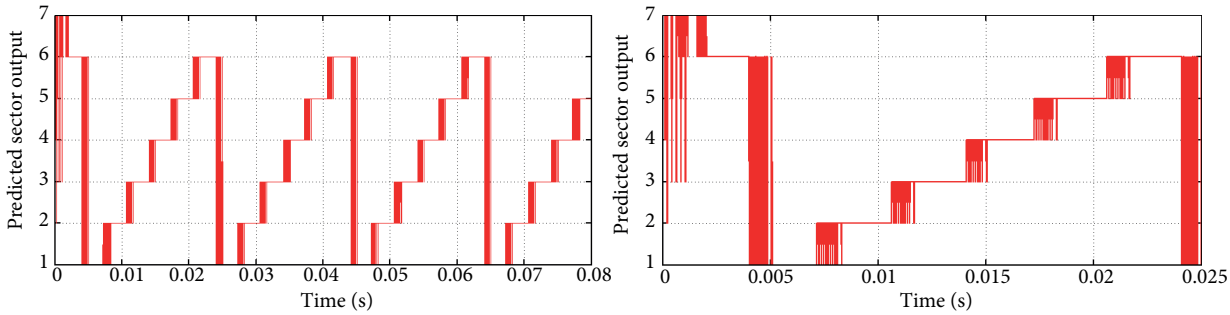

Figure 13. Vector selection process for the rectifier side based on MPC-DPC with the proposed switches sequence pattern.

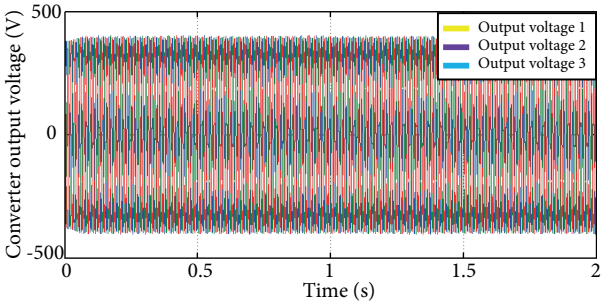

Figure 14. Controlled output voltages inverter side.

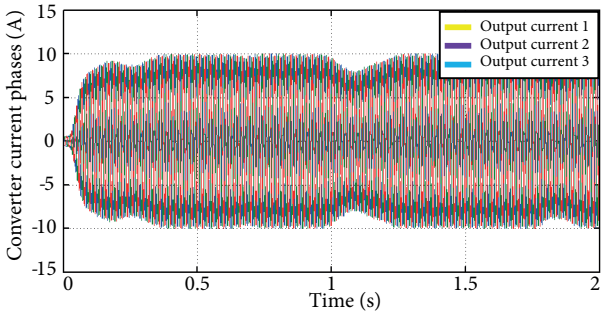

Figure 15. Output phase controlled currents.

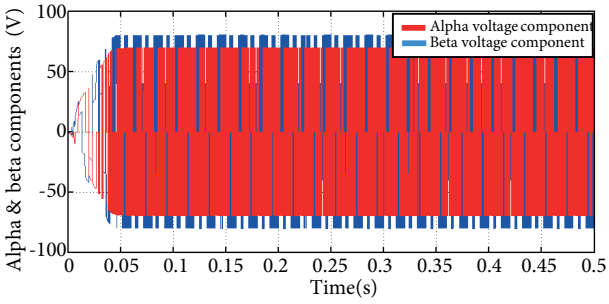

Figure 16. Alpha beta output voltages.

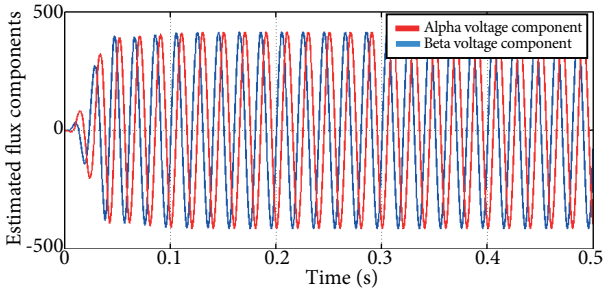

Figure 17. Output flux estimation using MVF.

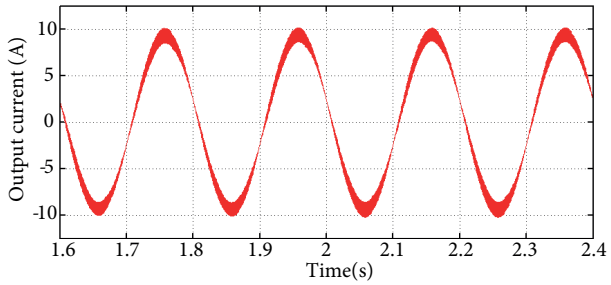

Figure 18. Input current with RL load and no input filter.

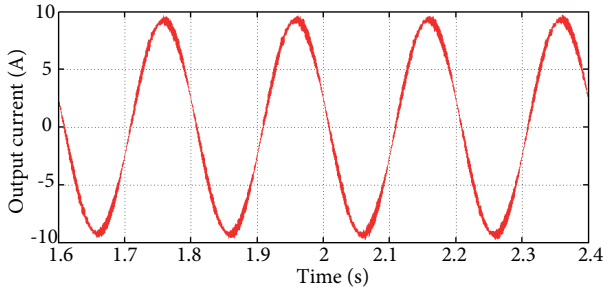

Figure 19. Input current with RL load and the designed input filter.

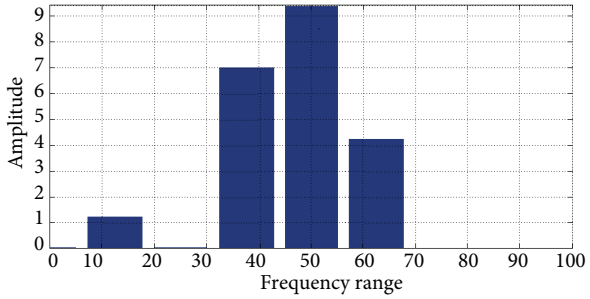

Figure 20. Spectral analysis for the input current with RL load and no input filter.

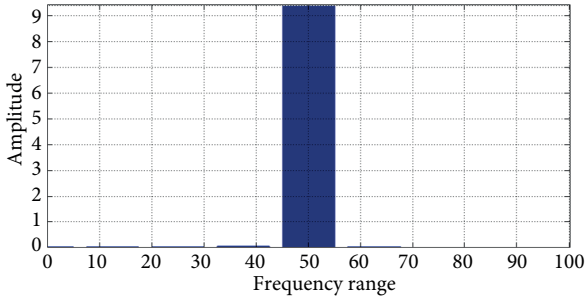

Figure 21. Spectral analysis for the input current with RL load and the designed filter.

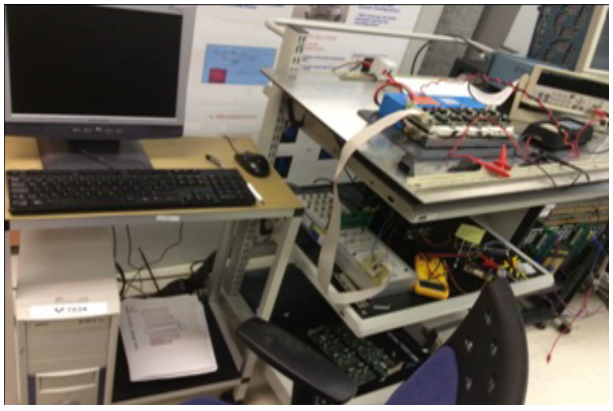

Figure 22. Experimental RT LAB platform with the power converter system.

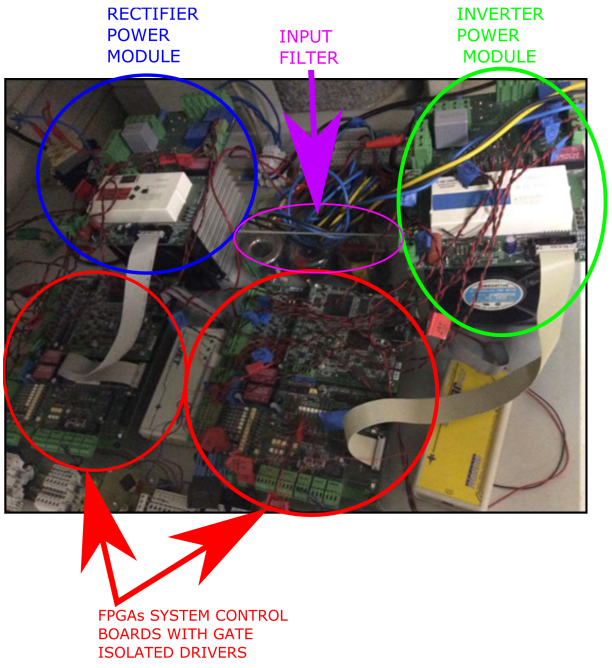

Figure 23. Experimental platform control system using FPGAs control cards.

The first results have been obtained with no input filter. Figure 26 illustrates that the proposed topology shows total control over the output converter current as the input one (Figure 27) with nearly unity power factor conditions on both sides.

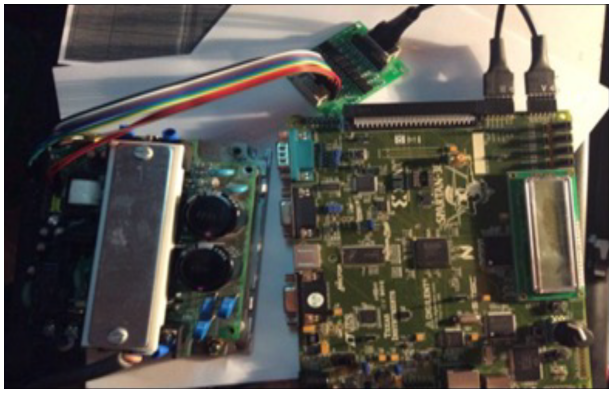

Figure 24. Power module rectifier test with FPGA control board.

Figure 25. Thermal camera screen capture for IGBT module skinny temperature test.

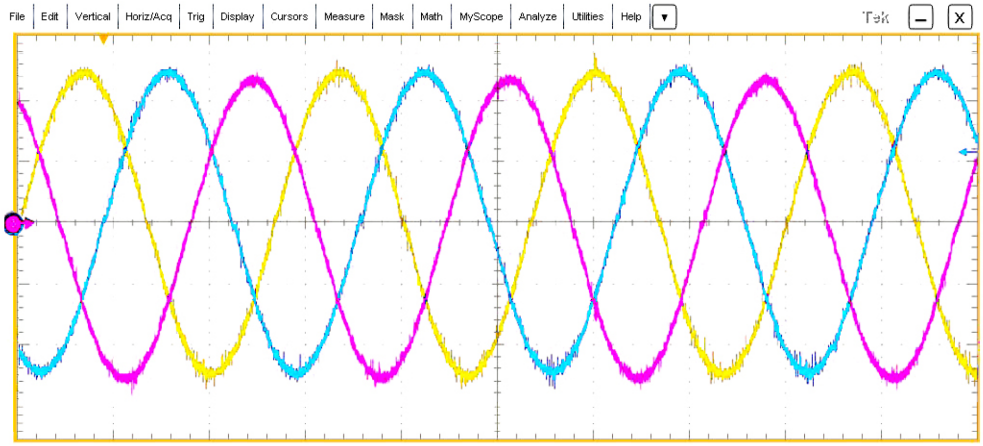

Figure 26. Converter output current system.

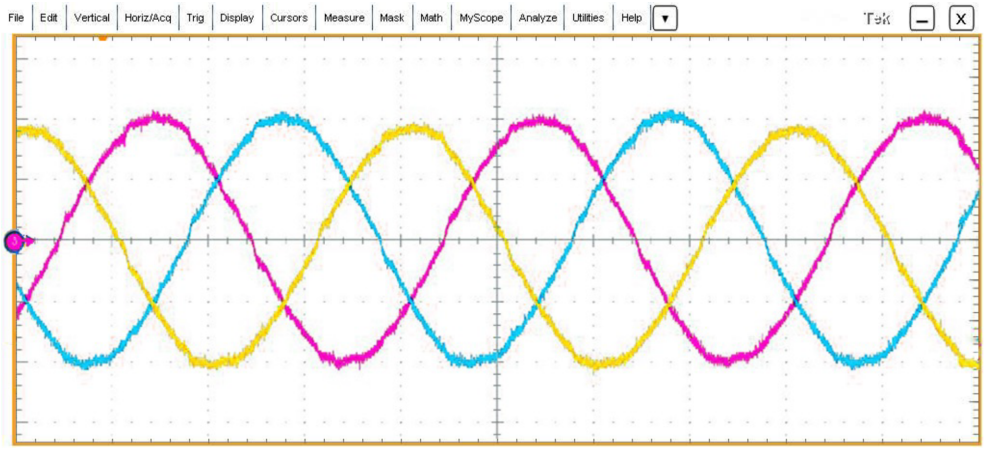

Figure 27. Converter system input currents.

5. Conclusion

The paper presents a novel control technique applied to a WTGS converter prototype based on two recent different control techniques to be applied for an offshore WTGS farm. A novel technique based MPC-DPC with a switching state table technique was improved and applied on both converters' sides. A thermal study and losses calculation are applied on the used power electronic modules to evaluate the performances of the proposed control topology technique. The obtained results demonstrate the high performances given by the built prototype, which can give a push to the proposed converter to be applied in a wide range in the WTGS world.

References

[1] Mattavelli P, Spiazzi G, Tenti P. Predictive digital control of power factor preregulators with input voltage estimation using disturbance observers. IEEE T Power Electr 2005; 20: 140-147.

[2] Rodriguez J, Pont J, Silva C, Salgado M, Rees S, Ammann U, Lezana P, Huerta R, Cortés P. Predictive control of three-phase inverter. Electronics Letters 29th April 2004.

[3] Kennel R, Linder A. Predictive control of inverter supplied electrical drives. IEEE T Power Electr 2000: 761-766.

[4] Cortés P, Ortiz G, Yuz JI, Rodríguez J, Vazquez S, Franquelo LG. Model predictive control of an inverter with output LC filter for UPS applications. IEEE T Ind Electron 2009; 56: 1857-1883.

[5] Linder A, Kennel R. Model predictive control for electrical drives. In: Proc. IEEE PESC 2005; Recife, Brazil: IEEE; pp. 1793-1799.

[6] Maciejowski JM. Predictive Control with Constraints. Englewood Cliffs, NJ, USA: Prentice-Hall, 2001.

[7] SidAhmeda T, Idir H, Mohamed El G, Scipioni A. Direct components extraction of voltage in photovoltaic active filter connected in a perturbed electrical network (based on robust PLL algorithm). International Conference on Technologies and Materials for Renewable Energy, Environment and Sustainability, TMREES15.

[8] Djazia K, Krim F, Sarra M. Active filter under unbalanced and distorted conditions. In: IEEE 2013 Power Eng & Optimization Conference (PEOCO); Langkawi: IEEE. pp. 664-669.

[9] Laib H, Kouara H, Chaghi A. A new approach of modulator active power filtering. International Journal of Advanced Science and Technology 2013: 50.

[10] Abdusalam M, Poure P, Saadate S. Hardware implementation of a three-phase active filter system with harmonic isolation based on self-tuning-filter. In: IEEE 2008 Power Electronics Specialists Conference 2008; IEEE. pp. 2875-2881.

[11] Karimi S, Poure P, Saadate S. High performances reference current generation for shunt active filter under distorted and unbalanced conditions. In: IEEE 2008 Power Electronics Specialists Conference 2008; IEEE. pp. 195-201.

[12] Casaravilla G, Salvia A, Briozzo C, Watanabe E. Control strategies of selective harmonic current shunt active filter. IEE Proceedings - Generation, Transmission and Distribution 2002. pp. 689-694.

[13] Lee KJ, Lee JP, Kim TJ, Yoo DW, Kwon SM, Kang DS, Kim HJ. A novel active power filter for selective harmonic suppression based on a robust PLL Algorithm; Proceedings - 2012 3rd IEEE International Symposium on Power Electronics for Distributed Generation Systems, PEDG 2012. pp. 416-422.

[14] Tadjer SA, Habi I, Nadji B. Study and simulation of active filtering of harmonic by method of synchronous reference frame. Proceedings of the International Conference on Power Engineering 2013, Energy and Electrical Drives, Turkey. pp. 1378-1381.

[15] Madaci M, Kerdoun D, Boumassata A, Cherfia N. Power active filter system implementation for photovoltaic generation system (PVGS) used in standing alone zones. 22–25 March 2014 (CEIT'14); Sousse, Tunisia. pp. 104-109.

[16] Vlatkovic V, Borojevic D, Lee F. Input filter design for power factor correction circuits. IEEE T Power Electr 1996; 11: 199-205.